镁合金真空电子束焊接匙孔热效应数值模拟

罗　怡[1,2]，刘金合[1]，叶　宏[2]
(1. 西北工业大学 材料学院，西安 710072；
2. 重庆理工大学 材料科学与工程学院，重庆 400050)

摘　要：分析了镁合金真空电子束焊接过程中的匙孔热效应特征，针对真空电子束焊接工艺建立了适用于镁合金焊接的复合热源模型。考虑到焊接过程中存在的高温金属蒸气等离子体及真空电子束焊接"匙孔"深熔效应特征，模型由高斯面热源和圆锥体热源复合而成，利用高斯面热源功率分配系数和圆锥体热源功率分配系数的不同取值，模拟电子束焊接的不同聚焦状态，并得到电子束聚焦状态与散焦状态下的焊接温度场变化，进而通过计算得到聚焦状态变化下的匙孔形状和焊缝成形。结果表明，模拟结果与其具有较好的一致性。

关键词：镁合金；真空电子束焊接；复合热源模型；匙孔热效应；焊缝成形
中图分类号：TG156　　文献标识码：A　　文章编号：0253-360X(2010)12-0073-04

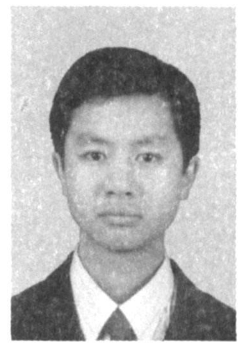

罗　怡

0 序　言

对于高功率密度的焊接热效应研究多是基于热传导理论。对于真空电子束焊接，基于热传导理论的热源模型主要有点热源、线热源和体热源。对于点热源与线热源的分析模型，虽具有一定的理论意义，但不能反映实际的焊接过程，还会在焊缝模型的中心线上产生歧义。因此，目前体热源在高功率密度焊接方法的数值模拟中具有较为广泛的应用[1-4]。

文中即是针对镁合金的真空电子束深熔焊接热效应进行的数值模拟研究。在真空电子束深熔焊接镁合金的过程中，电子束热源一方面产生匙孔效应，获得深熔焊接效果；另一方面，由于镁合金中如 Mg，Zn等元素沸点低，在高功率密度的热源作用下伴随强烈的蒸发现象，形成高温金属蒸气等离子体，在压力梯度的作用下喷出匙孔[5]。可见，匙孔效应使镁合金真空电子束焊接过程的热效应不同于普通熔化焊接，并对焊缝成形造成了显著的影响[6-8]。为了在研究中更接近于实际的热效应特征，采用高斯表面热源与圆锥体热源复合的热源模型来模拟这种深熔焊接效果，研究不同的电子束聚焦状态下的匙孔热效应特征和对焊缝成形的影响。

收稿日期：2009-08-17
基金项目：重庆市教委科学技术研究资助项目(KJ100826)；江苏科技大学先进焊接技术省级重点实验室开放研究基金资助项目

1 匙孔热效应分析

真空电子束焊接热源具有高能量密度的特点，这是产生匙孔效应的能量基础。图 1为真空电子束焊接过程示意图。图中 B为熔宽，H为熔深。在焊接过程中，被聚焦的电子束流高速撞击金属材料表面，电子的动能瞬间转换为热能，并在焊接热源作用初期加热材料表面。在这种作用下，电子束热源作用的金属材料的熔池固液界面处的温度迅速升高，由于高功率密度的电子束热源的加热速率极高，使熔池表层温度上升速率极快，当熔池表面向材料内部传递的热量远低于表层的热量时，表层材料温度升高，一些低熔点的金属元素开始蒸发。电子束的能量足以击穿金属蒸气使之电离，即形成金属蒸气等离子体。只要入射电子束的能量不低于激发金属材料形成等离子体的电子束能量，等离子体的形成

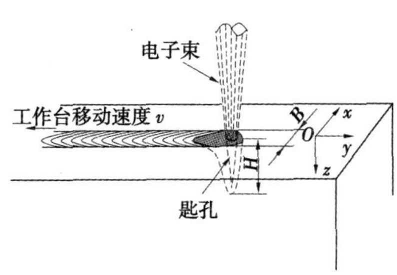

图 1　真空电子束焊接示意图
Fig. 1　Schematic diagram of vacuum electron beam welding

将维持连续. 蒸发效应产生的反作用力将排开熔化金属, 使电子束流可以直接作用于熔池底部, 同时, 蒸发产生的蒸气压力也会维持匙孔的形成. 这就是真空电子束焊接匙孔效应下的直接作用机制.

从金属材料蒸发过程发生的瞬间开始, 材料表层以及金属气相的温度将由蒸发机制来控制, 相对于该机制, 向熔池内层的热传导作用不再显著. 等离子体将继续吸收电子束能量而维持高温状态, 在不断喷出过程中, 在焊缝表面达成局部压力平衡, 从而形成特殊的表面热源. 这样, 焊接过程中的材料不断蒸发产生的蒸气流作用, 使高功率密度的电子束流可以在极短时间内形成大深宽比的焊缝.

由分析可见, 匙孔效应的产生及其发展、变化与电子束流的能量分布状态关系密切. 如图 2所示, 经过高电压聚焦的电子束流聚焦点两侧存在一个近场区, 即电子束的活性区间 (depth of field, DOF). 在这个区间内, 电子束流的直径变化不大, 且具有最大的功率密度分布. 沿深度方向偏离电子束活性区间, 随着电子束半径的增大、电子散射的加强、与材料交互作用物理效应下能量的吸收, 电子束的功率密度递减, 其热效应大大降低. 由此可见, 电子束活性区间附近的能量分布呈现高斯规律变化, 电子束聚焦状态的变化对匙孔热效应的影响将形成不同的温度场分布和焊缝成形.

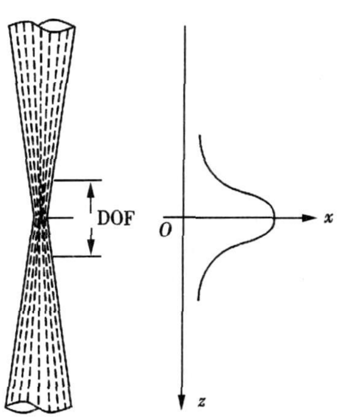

图 2 电子束活性区间及其能量分布

Fig. 2 Depth of field and energy distribution of electron beam

2 匙孔热效应计算模型

图 3为建立的适用于镁合金真空电子束焊接的复合热源模型. 匙孔效应产生的深熔热效应是在极高功率密度电子束热源作用下产生的, 采用三维圆锥体热源模拟这种焊接效果. 另一方面, 在真空焊接环境下, 焊缝表面形成局部压力平衡的高温金属蒸气等离子体具有面热源的特征, 采用高斯面热源模拟这种表面热效应, 使真空电子束焊缝形成较大的开口. 即建立高斯面热源与圆锥体热源复合的热源模型来实现镁合金的真空电子束深熔焊接模拟.

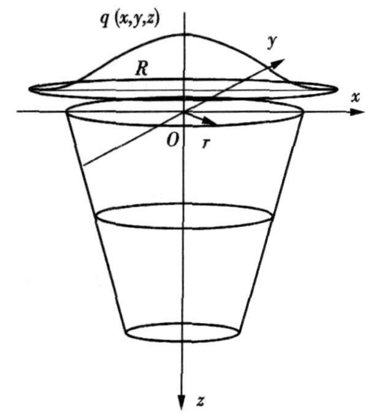

图 3 复合热源模型

Fig. 3 Model of composite heat source

对于高斯面热源, 其热流密度分布为

$$q_s(x,y)=\frac{3Q_s}{\pi R^2}\cdot\exp\left[-\frac{3(x^2+y^2)}{R^2}\right] \tag{1}$$

式中: $q_s(x,y)$为笛卡儿坐标系内任一位置处的焊接热源功率密度分布; Q_s为高斯面热源功率; R为高斯面热源作用半径. 并且, 根据旋转体的坐标特征, $x^2+y^2=r^2$, r为一点到热源中心的径向距离.

对于圆锥体热源, 其热流密度分布为

$$q_V(x,y,z)=\frac{9Q_V}{\pi h r_0^2}\cdot\exp\left[-\frac{h^2}{(h-z)^2}\cdot\frac{3(x^2+y^2)}{r_0^2}\right] \tag{2}$$

式中: Q_V为圆锥体热源功率; h为电子束热源的有效作用深度; r_0为热源作用在表面时的半径; z的取值范围为 $(0, h)$.

两种热源的功率之和与焊接的有效热输入功率相等, 即

$$Q_s+Q_V=Q \tag{3}$$

式中: Q为焊接有效热输入功率, 其表达式为

$$Q=CU_aI_b \tag{4}$$

式中: C为电子束热源有效功率系数, U_a为加速电压; I_b为焊接束流.

高斯面热源所占焊接有效热输入功率的功率分配系数为 γ_S, 圆锥体热源所占焊接有效热输入功率的功率分配系数为 γ_V, 且 $\gamma_S+\gamma_V=1$, 则有

$$Q_s=\gamma_S Q \tag{5}$$

$$Q_V=\gamma_V Q \quad (6)$$

分配系数 γ_S, γ_V 可以表征不同聚焦状态下, 焊缝沿深度方向的能量分布规律变化, 即聚焦状态时, 圆锥体热源的功率分配系数 γ_V 占较大比例, 使圆锥体热源在匙孔热效应的模拟中为主要热源, 表征较高的电子束热源能量密度作用下, 形成深熔焊接的效果; 而散焦状态时, 高斯面热源的功率分配系数 γ_S 所占比例增加, 可凸显低能量密度电子束热源作用下的熔化效应. 这样也在一定程度上反映了不同聚焦状态下的焊缝横截面的形貌特征, 如焊缝深宽比参数等.

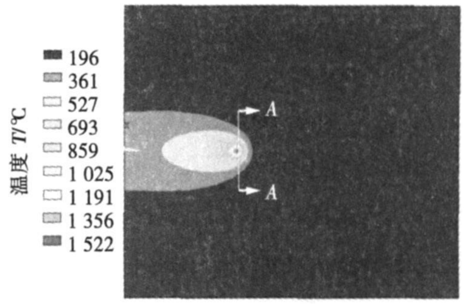

图 4　AZ61镁合金电子束焊接温度场

Fig. 4　Welding temperature field for AZ61 magnesium alloy

3　计算结果及讨论

3.1　焊接温度场

采用 AZ61镁合金材料的热物理性能参数进行相应的焊接热效应计算及数值模拟, 并采用该材料进行焊接试验. 图 4为利用建立的复合焊接热源进行数值模拟得到的 AZ61镁合金真空电子束焊接的温度场分布, 焊接工艺参数为加速电压 $U_a=60$ kV, 焊接束流 $I_b=30$ mA, 焊接速度 $v=18$ mm/s, 电子束的聚焦状态为表面聚焦, 即 $\gamma_S=0.1$, $\gamma_V=0.9$.

在图 4中, 沿 "A—A" 方向可以计算焊缝横截面温度场分布. 图 5为聚焦状态下和散焦状态下的焊缝横截面温度场. 为了利用焊接复合热源模型实现不同的聚焦状态, 面热源功率分配系数 γ_S 和体热源功率分配系数 γ_V 分别取不同值, 即聚焦状态时 $\gamma_S=0.1$, $\gamma_V=0.9$ (图 5a); 散焦状态时 $\gamma_S=0.3$, $\gamma_V=0.7$ (图 5b) 和 $\gamma_S=0.4$, $\gamma_V=0.6$ (图 5c).

可以看出, 聚焦状态下, 圆锥体热源为焊接主要热源; 散焦状态下, 随着散焦程度的增加, 高斯面热源所占比例逐步增加. 采用这样的能量分配原则, 可以模拟出电子束活性区不同的偏离程度下, 对焊接温度场的影响. 图 5a情况下, 电子束活性区位于工件表面或近表面, 获得深穿透的焊接效果和较高的温度分布. 图 5b, c情况下, 电子束活性区逐步远离焊缝表面, 获得相对较浅的穿透效果和较低的焊接温度场分布.

3.2　匙孔变化及焊缝成形

在图 5中采用的能量分配情况下, 对焊接过程的匙孔变化和焊缝成形有显著影响. 由于此处对于匙孔的形成主要考虑电子束穿透过程中, 高温金属蒸气的效应, 因此, 近似设定 Mg元素的沸点为门限值计算匙孔形状, 匙孔内的高温金属蒸气等离子体温度远高于该门限值, 研究中忽略匙孔内高温的金属蒸气相传热效应. 计算区域中, 高于蒸发门限值的区域视为匙孔区. 试验采用的镁合金为 AZ61镁合金, 以其熔点为门限值计算焊缝成形, 如图 6所示. 计算区域中, 高于熔化门限值的区域视为焊缝区. 可以看出, 图 5a的聚焦状态下, 得到深穿透的焊接效果, 匙孔基本贯穿计算板厚, 获得的焊缝形状也完全穿透. 图 5b的散焦状态下, 由于散焦程度的不同, 匙孔显著减小, 且无法贯穿计算板厚, 这也影响了焊缝成形.

图 7为三种聚焦状态下的试验焊缝. 焊接工艺参数为加速电压 $U_a=60$ kV, 焊接束流 $I_b=30$ mA, 焊接速度 $v=18$ mm/s. 图 7a采用的聚焦电流 (I_f) 为 470 mA, 图 7b采用的聚焦电流为 465 mA, 图 7c

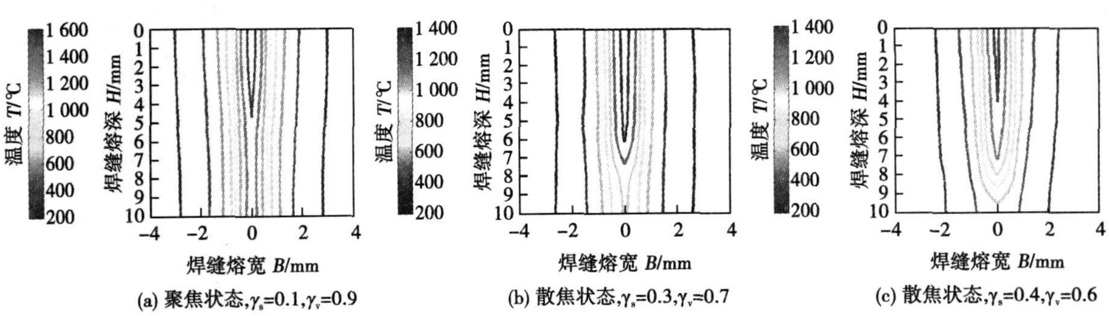

图 5　不同聚焦状态下的焊缝横截面温度场

Fig. 5　Temperature fields of weld cross-section in various focus states

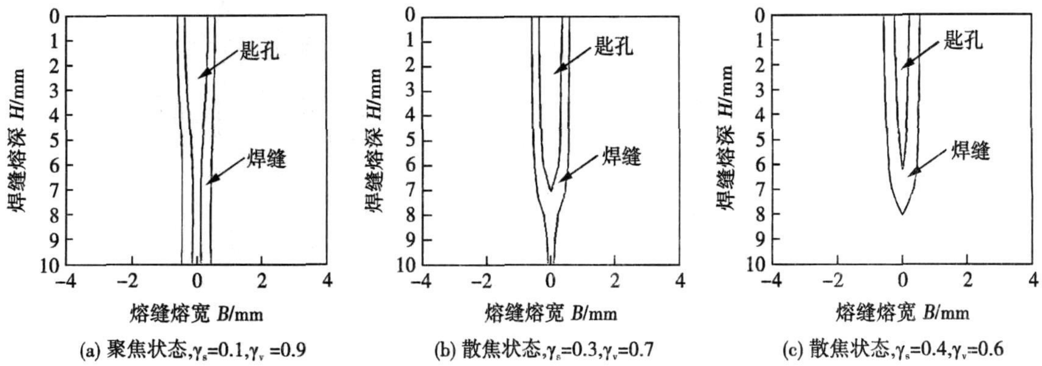

图 6 不同聚焦状态的匙孔变化及焊缝成形模拟

Fig. 6 Simulation shapes of keyholes and welds in various focus states

采用的聚焦电流为 460 mA,可见聚焦电流对焊缝成形的显著影响,这基本可以验证图 6中各图的焊缝成形.

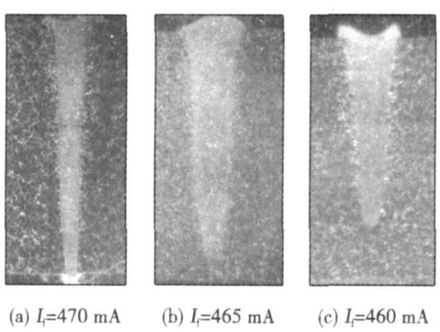

图 7 不同聚焦状态下的焊缝成形

Fig. 7 Welds shape of in various focus states in experiments

4 结 论

(1)建立了高斯面热源与圆锥体热源复合的焊接热源模型,高斯面热源实现了对匙孔热效应下的高温金属蒸气熔化效果的模拟,圆锥体热源实现了对匙孔深穿透效应的模拟,计算得到的温度场分布符合实际焊接情况.

(2)用功率分配系数决定两种热源的能量分配,实现了对不同的电子束聚焦效果的模拟,获得复合实际焊接情况的匙孔变化规律和焊缝成形,同时也可以看出聚焦电流对匙孔热效应的影响,进而影响焊接质量.

参考文献:

[1] Ho C Y, Wen M Y, Lee Y C. Analytical solution for three-dimensional model predicting temperature in the welding cavity of electron beam[J]. Vacuum, 2008, 82(3): 316—320.

[2] Liang G L, Zhou G, Yuan S Q. Study on hybrid heat source overlap welding of magnesium alloy AZ31B[J]. Materials Science and Engineering A, 2009, 499(1/2): 93—96.

[3] Paolo F, Andrea Z, Franco B. Investigation of electron-beam welding in wrought inconel 706-experimental and numerical analysis[J]. Materials Science and Engineering A, 2005, 392(1/2): 94—105.

[4] Gery D, Long H, Maropoulos P. Effects of welding speed, energy input and heat source distribution on temperature variations in butt joint welding[J]. Journal of Materials Processing Technology, 2005, 167(2/3): 393—401.

[5] Peter P, Chavdar G, Georgy P. Experimental investigation of weld pool formation in electron beam welding[J]. Vacuum, 1998, 51(3): 339—343.

[6] Mladenov G, Vutova K, Wojcicki S. A study of weldability and fracture modes in electron beam weldments of AZ series magnesium alloys[J]. Vacuum, 1998, 51(2): 231—233.

[7] Koleva E, Mladenov G, Vutova K. Calculation of weld parameters and thermal efficiency in electron beam welding[J]. Vacuum, 1999, 53(1/2): 67—70.

[8] Koleva E. Electron beam weld parameters and thermal efficiency improvement[J]. Vacuum, 2005, 77(4): 413—421.

作者简介:罗 怡,男,1979年出生,博士研究生,讲师.主要研究方向为焊接方法及自动化.发表论文 20余篇.

Email: luoyi@cqut.edu.cn

Microstructures and properties of SiC_w/**2024**Al MMCs joint by capacitor discharge welding XU Feng, ZHAI Qiuya, XU Jinfeng (1. School of Material Science and Engineering, Shaanxi University of Technology, Hanzhong 723003, China; 2. School of Material Science and Engineering, Xi'an University of Technology, Xi'an 710048, China). p 57—60

Abstract: The capacitor discharge spot welding on SiC_w/2024Al alloy matrix composite sheet with 0.2 mm thickness was study. The microstructures and properties of the joint were analyzed, and the temperature field and cooling rate of nugget were calculated. The results show that the joint microstructure consists of nugget zone, heat-affected zone and semi-melt zone. The cooling rate of the joint reaches to 5.25×10^6 K/s. The microstructure of the nugget is obviously refined and the SiC-Al interfacial reaction is not found in the middle of the joint because of high cooling rate. The width of semi-melt zone is 10 to 15 μm, which divides the nugget zone and base metal. The microstructure of heat-affected zone is not obviously coarse and keeps conformation with base metal. To obtain the high quality spot weld joint, the welding parameters are a welding voltage of 80 V, a capacitor of 3 300 μF and a electrode pressure of 18 N.

Key words: composite material; SiC whisker reinforced Al alloy matrix composites; capacitor discharge welding; microstructures and properties of joint

Robust joint tracking with structured-light vision sensing GONG Yefei, DAI Xianzhong, LI Xinde, ZHANG Jie (Key Laboratory of Measurement and Control of Complex Systems of Engineering, Ministry of Education, Southeast University, Nanjing 210096, China). p 61—64

Abstract: The performance of joint feature extraction is degraded greatly during welding because of severe disturbances, so a prediction-matching-estimation combined close-looped iterated method is proposed for weld feature tracking. The position and shape of the joint stripe profile in the image is predicted at first, then the joint is recognized by a model-based profile matching method, and lastly the weld trajectory is filtered and estimated based on the confidence of the extracted feature. Experiments show that the method promotes the joint recognition results to ensure a robust and real-time weld seam tracking even in the face of gross error or failure occurrence in joint feature extraction.

Key words: joint tracking; structured-light vision; prediction; filtering

High-temperature oxidation behavior of cerium on the surface of Sn-Zn lead-free solders WANG Hui, LIU Xincai, PAN Jing, MA Yongcun (Faculty of Materials Science and Chemical Engineering, Ningbo University, Ningbo 315211, China). p 65—69

Abstract: The distribution and existing form of Ce on the surface of Sn-9Zn-0.15Ce and Sn-9Zn-0.002Al-0.2Ga-0.25Ag-0.15Ce solder are investigated by atomic emission spectrometry and X-ray photoelectron spectroscopy. Results indicate that Ce enriches on the surface of the Sn-9Zn-0.15Ce solder in the range of 0 to 40 nm. The concentration of Ce in the enriched zone is about 30 at%, which is 250 times of that in the bulk solder, and the enriched Ce on the surface is mostly oxidized as CeO_2 and Ce_2O_3. With the multi-addition of Ga and Al in the Sn-9Zn-0.002Al-0.2Ga-0.25Ag-0.15Ce solder, Ga enriches in range of 0 to 6 nm on the surface, while Al enriches in range of 2 to 20 nm in oxidized form. The Ce-enriched layer is in the range of 2 to 60 nm on the surface covered by the Ga and Al enriched layers, and the oxidation of Ce is depressed significantly.

Key words: Sn-Zn; lead-free solder; Ce; oxidation; surface enrichment

Influence of ceria on phosphorus and sulphur of low alloy steel weld FAN Xiying, GUO Yonghuan (College of Mechanical and Electrical Engineering, Xuzhou Normal University, Xuzhou 221116, China). p 70—72

Abstract: The coating of E5515-G, a low alloy steel electrode, was added in different amount of ceria (CeO_2) for enhancing electrode properties which was studied by means of impact toughness, metallographic examination and X-ray fluorescence spectrometry test. The results show that the proper addiction of CeO_2 is beneficial to the desulfurization and dephosphorization of the weld and improves the impact absorbed energy of deposited metal. Different addition amount of CeO_2 can lead to various desulfurization efficiency, which makes a great difference, whereas the dephosphorization efficiency is unconspicuous. The microstructures of the weld can be effectively made fine by adding CeO_2 into electrode coating, but the addition amount of CeO_2 should be proper. The microstructure of the weld is the finest when the addition amount of CeO_2 is 3%. When the amount of CeO_2 is optimal, the S content in weld metal will decrease by 58.128 1%, while the P content 14.285 7%.

Key words: ceria; low alloy steel electrode; weld; sulphur; phosphorus

Numerical simulation on keyhole thermal effect of vacuum electron beam welding of magnesium alloy LUO Yi[1,2], LIU Jinhe[1], YE Hong[2] (1. School of Material Science and Engineering, Northwestern Polytechnical University, Xi'an 710072, China; 2. School of Material Science and Engineering, Chongqing Institute of Technology, Chongqing 400050, China). p 73—76

Abstract: The keyhole thermal effect of vacuum electron beam welding for magnesium alloy was analyzed. In view of the thermal effect of high-temperature metal vapor and the deep-penetration effect of keyhole during welding, a composite heat source model applying to magnesium alloy, which was made up of Gaussian surface source and cone body source, was developed. By the different valuation to the power coefficients of Gaussian surface source and cone body source, the various focus states of electron beam were simulated to get the welding temperature fields. And then, the simulation results were favorable for the shape calculation to keyholes and welds. The experimental results show that the simulation results have good consistency with the experiment welds.

Key words: magnesium alloy; vacuum electron beam welding; composite heat source model; keyhole thermal effect; weld shape

Damage of two-spot welds under two level loading WANG Ruijie[1], SHANG Deguang[1], LIU Hongbin[1] (1. Faculty